

University of South Dakota

USD RED

Honors Thesis

Theses, Dissertations, and Student Projects

Spring 5-2-2023

HOLLOW Mn₃O₄ NANOPARTICLES FOR CATALYTIC OXIDATION OF ALKENES IN AIR

Nathan R. Loutsch

University of South Dakota

Follow this and additional works at: <https://red.library.usd.edu/honors-thesis>



Part of the [Inorganic Chemistry Commons](#), and the [Materials Chemistry Commons](#)

Recommended Citation

Loutsch, Nathan R., "HOLLOW Mn₃O₄ NANOPARTICLES FOR CATALYTIC OXIDATION OF ALKENES IN AIR" (2023). *Honors Thesis*. 307.

<https://red.library.usd.edu/honors-thesis/307>

This Honors Thesis is brought to you for free and open access by the Theses, Dissertations, and Student Projects at USD RED. It has been accepted for inclusion in Honors Thesis by an authorized administrator of USD RED. For more information, please contact dloftus@usd.edu.

HOLLOW Mn₃O₄ NANOPARTICLES FOR
CATALYTIC OXIDATION OF ALKENES IN AIR

by

Nathan Roy Loutsch

A Thesis Submitted in Partial Fulfillment
Of the Requirements for the
University Honors Program

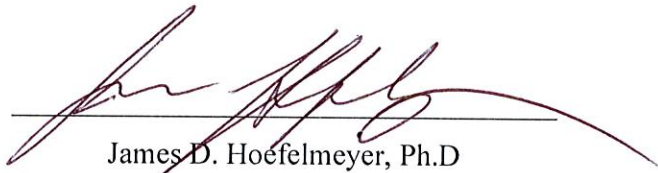
Department of Chemistry
The University of South Dakota

May 2023

The members of the Honors Thesis Committee appointed

to examine the thesis of Nathan Roy Loutsch

find it satisfactory and recommend that it be accepted.



James D. Hoefelmeyer, Ph.D

Professor of Chemistry

Director of the Committee



Steven Wu, Ph. D

Assistant Professor of Chemistry



Catalin Georgescu

Associate Professor of Mathematics

ABSTRACT

HOLLOW Mn_3O_4 NANOPARTICLES FOR CATALYTIC OXIDATION OF ALKENES IN AIR

Director: James Hoefelmeyer, Ph.D.

Oxidized hydrocarbons (epoxides, alcohols, carboxylic acids, ketones, and aldehydes) have many uses including fuel production, pollution treatment, and chemical synthesis. These compounds can be formed by oxidizing alkenes and alkanes with the assistance of a catalyst. Heterogeneous catalysts have greater recyclability, but traditionally have lower activity and selectivity. Due to the increased relative surface area, nanomaterials can overcome some of the physical limitations. The Hoefelmeyer lab developed a new nanomaterial: hollow Mn_3O_4 nanoparticles. Sensitive synthetic conditions have been optimized. Due to the increased relative number of edge and corner atoms, the reactive properties of most small nanomaterials increase. Because of the catalytic nature of bulk manganese oxides, the catalytic properties of the new particles with unique morphology are being tested. The hollow structure may provide more active sites due to increased surface area with an internal cavity potentially available for catalytic sites. Preliminary investigation of oxidative catalysis with a select few alkenes: cyclohexene, trans-stilbene, and toluene shows some promise.

Keywords: Heterogeneous Catalysis, Ketone Formation, Hollow Nanoparticles, Cyclohexene, Catalyst Design.

TABLE OF CONTENTS

List of Figures	vi
List of Tables	vii
Acknowledgements	viii
Chapter One: Introduction	1
1.1 Objective	1
1.2 Catalysis	1
1.2.1 Nanomaterial Catalysis	3
Chapter Two: Methods	5
2.1 Nanoparticle Synthesis	5
2.1.1 MnO Synthesis	5
2.1.2 Mn ₃ O ₄ Synthesis	6
2.2 Catalysis	6
2.2.1 Procedure	6
2.2.2 GC-MS Method File	8
Chapter Three: Results and Discussion	10
3.1 Characterization of MnO and Mn ₃ O ₄	10
3.1.1 MnO NPs	11
3.1.2 Mn ₃ O ₄ NPs	14
3.2 Catalysis	17
3.2.1 Cyclohexene Oxidation	17

3.2.2 Trans-Stilbene Oxidation	20
3.2.3 Toluene Oxidation	21
Chapter Four: Conclusion	23
Bibliography	24

LIST OF FIGURES

1.1 Catalysis Diagram	2
1.2 Hausmannite Crystal Structure	4
2.1 Gas Chromatography Method File	8
2.2 Mass Spectrometry Method File	9
3.1 PXRD of MnO	12
3.2 TEM of MnO	12
3.3 Histogram of MnO nanoparticle sizes	13
3.4 PXRD of hollow Mn ₃ O ₄ nanoparticles	14
3.5 TEM of hollow Mn ₃ O ₄ nanoparticles	15
3.6 Histograms of hollow Mn ₃ O ₄ nanoparticle sizes	16
3.7 GC-MS of Cyclohexene Room Temperature Catalysis in Hexane	17
3.8 GC-MS of Cyclohexene Room Temperature Catalysis in THF	18-19
3.9 GC-MS of Trans-stilbene 40°C Catalysis with O ₂	20
3.10 GC-MS of Toluene Room Temperature Catalysis with O ₂	21

LIST OF TABLES

1.1 Safety Aspects of various oxidants for alkenes.	2
3.1 Notable Peaks from Figure 3.7	18
3.2 Notable Peaks from Figure 3.8	19
3.3 Notable Peaks from Figure 3.9	20
3.4 Notable Peaks from Figure 3.10	22

ACKNOWLEDGEMENTS

I would like to extend my thanks to

Dr. Hoefelmeyer, for your continued support and guidance of my growth and education. I had the privilege of being a member of your group for the last year and a half of my undergraduate degree. You are an excellent teacher, mentor, and role model. You have an unmatched passion for chemistry that is inspiring.

Dr. Wu, my first research mentor. You first got me interested in research and nanomaterials. I got to work on projects with copper nanoclusters and mesoporous silica nanoparticles. You helped push me in the path of becoming a scientist and helped me to develop the skills I will need to succeed in the field.

Dr. Georgescu, the final member of my thesis committee. Your continued support, inside and outside the classroom has been beneficial to my growth as a student and researcher.

Pranab Kumar Nandy, my lab partner. Without you, this project would not have been possible. You have helped teach me many practical skills for research that cannot be learned in a class. I have enjoyed working with you on this project, and I hope you have a successful career

My friends, family, and colleagues for your continued support. Special thanks to my parents, Marie and Jeffrey. You have always encouraged me to pursue my interests in academics, research, and life. Though you are not scientists, you are always interested in hearing about my research.

The chemistry faculty at USD. The last four years have felt like I have been the member of a close-knit family. Special Thanks to Dr. Vlasisavljevich, my graduate advisor, for your support, input, and willingness to juggle my hectic workload as an accelerated master's student.

CHAPTER ONE

Introduction

1.1 Objective

Catalytic oxidation reactions introduce oxygen to hydrocarbons. Fuel production¹, pollutant treating²⁻⁴, and many chemical syntheses⁵ are all achieved through catalytic oxidation. Alkanes and alkenes can be converted into many useful intermediates like ketones, aldehydes, carboxylic acids, alcohols, and epoxides.

Many oxidizers can be used including oxygen, meta-chloroperoxybenzoic acid (mCPBA), peracetic acid, and hydrogen peroxide. Harsher oxidizers like hydrogen peroxide often come with safety concerns. They can be difficult to acquire, handle, and dispose of. Many can even be harmful to humans. This makes them difficult to work with and less desirable for use in industry and research. A list of common oxidants and their safety concerns is summarized in Table 1.1.

Concentrated molecular oxygen (O_2) as well as the oxygen present in air are desirable to use as oxidants. Unlike harsher oxidants, molecular oxygen can be a safe, cheap, reliable source for oxidation. However, oxygen is a relatively stable molecule. The kinetics of alkene oxidations in concentrated oxygen or air can require a large activation energy (E_a)^{6, 7}. Many reactions require high temperatures to be favorable even under catalysis.

1.2 Catalysis

To make a reaction more energetically favorable, a catalyst is often used. This lowers the activation energy or energy barrier. It does not change the difference in energy

between the reactants and products or Gibbs Free Energy (ΔG). Figure 1.1 shows how this barrier may be reduced. The quality of a catalyst is often determined by how efficiently convert reactant(s) to product(s) per active site. Inexpensiveness, nontoxicity, stability, recyclability, and selectivity are desirable traits for a catalyst. Use of mild conditions (short time at room temperature) are also ideal.

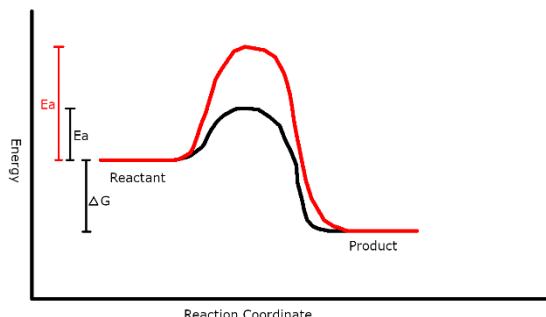


Figure 1.1. Qualitative free energy diagram for a catalyzed reaction

Red, taller curve serves as the potential energy surface for an uncatalyzed reaction. The black, shorter curve serves as the potential energy surface for the catalyzed reaction. ΔG does not change for the reactions, but E_a does.

Table 1.1: Safety Aspects of Various Oxidants for Alkenes

Reproduced from [1] with permission.

Compounds	Safety Aspects
H ₂ O ₂ (30%)	Corrosive to the eyes, skin, and respiratory system.
tBuOOH (70 wt% in water)	Exceptionally dangerous, highly reactive, flammable, and toxic. Corrosive to skin and mucous membranes and causes respiratory distress when inhaled.
CmOOH (80% tech. grade)	Breathing Cumene Hydroperoxide can irritate the lungs causing coughing and/or shortness of breath, headache, dizziness, poor coordination and even passing out.
Peracetic acid (32 wt%)	Corrosive/irritating to the eyes, mucous membranes of the respiratory tract, and skin to concentrations as low as 5 ppm.
mCPBA (77 wt%)	Irritates the mucous membranes, respiratory tract, eyes and skin. Moreover, skin contact with mCPBA causes burns and blisters.

There are two types of catalysts: heterogeneous and homogeneous. Homogeneous catalysts are in the same phase as the reactant(s) whereas heterogeneous catalysts are not. For example, a solid catalyst in a liquid would be a heterogeneous catalyst. A polar, liquid

catalyst in water would be a homogenous catalyst. Several heterogeneous⁸⁻¹¹ and homogeneous¹²⁻¹⁴ catalysts have been developed for alkene oxidation.

Heterogeneous catalyst are easier to separate while homogeneous catalysts tend to have higher activity and selectivity¹⁵. Because of the easy of separability for heterogeneous catalysts, they can have greater recyclability. Heterogeneous catalysts have physical limitations to their activity. Reactions can only occur at the interfaces where the catalyst meets the reactant. To overcome this, one solution is to use a higher surface area material as a catalyst. This provides more active sites for catalysis to occur.

1.2.1 Nanomaterial Catalysis

Nanomaterials are ideal for catalysis. Nanomaterials have a high surface area to volume ratio. Nanoparticles have high tunability of their size, shape, and composition¹⁶. Nanoparticles have a higher loading capacity and more uniform dispersion compared to traditional catalysts. However, they are prone to agglomeration (clumping) and may have increased preparation time or cost.

Recently, our group discovered a synthesis method for hollow Mn_3O_4 nanoparticles. These NPs have a unique morphology that have been achieved in other metal oxide materials^{17, 18}. The increased number of active sites from the morphology gives the potential for the H- Mn_3O_4 NPs to have a high activity.

Our Mn_3O_4 nanoparticles share the structure of a naturally occurring crystal. Hausmannite belongs to a family of crystals with a tetragonal lattice. In the tetragonal lattice, all of the angles of a unit cell are the same ($\alpha=\beta=\gamma=90^\circ$). Two of the side lengths (a and b) of the unit cell are equivalent, while the third is unique ($a=b\neq c$). For hausmannite, $a=5.76 \text{ \AA}$, $c=9.46 \text{ \AA}$, and of course, $\alpha =90^\circ$. Figure 1.2 shows the structure of hausmannite.

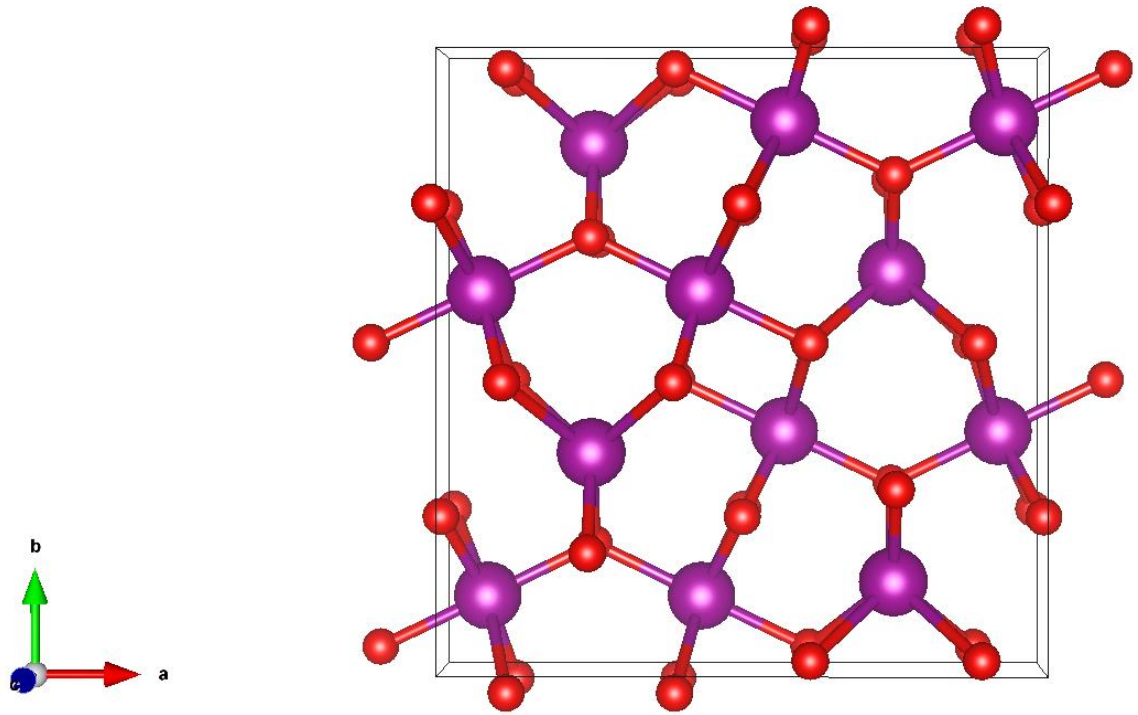


Figure 1.2: Hausmannite Structure.

Perspective image of the tetragonal structure of hausmannite (Mn_3O_4)

CHAPTER TWO

Methods

2.1 Nanoparticle Synthesis

2.1.1 Synthesis of MnO

Synthesis of the MnO followed the Hyeon group's method¹⁹ as previously performed by Hoefelmeyer group²⁰. $\text{MnCl}_2 \cdot 4\text{H}_2\text{O}$ (7.91 g, 25 mol) and sodium oleate (36.5 g, 8.34 mol) were added to a 1 L round bottom flask with "nanopure" 18.2 M Ω water (60 mL), ethanol (80 mL), and hexanes (140 mL). This mixture was heated to 65°C for 4 hours before cooling to room temperature. The contents settled into organic and aqueous layers. These were washed and separated thrice with 30 mL water. The organic solution containing the manganese (II) oleate was transferred to a new 1 L three-neck round bottom flask. Solvent was removed in vacuo and left a brown waxy residue. Degassed oleic acid (6.3 mL) and degassed 1-octadecene (250 mL) were added to the flask. A reflux condenser was fitted. The contents were heated at a rate of 3.3°C/min, held at 320°C for 30 min, and allowed to cool back to room temperature. Under inert atmosphere, the contents were off-white, but became dark brown when exposed to air. This is due to oxidation of the surface of the MnO into a thin Mn_3O_4 layer. Isopropanol (200 mL) was added to induce precipitation of the nanoparticles. The mixture was centrifuged at 3500 rpm for 8 min. The supernatant was discarded. Isolated, purified MnO nanocrystals were redispersed in hexanes (40 mL). Concentration is determined by taking a 1 mL aliquot. The aliquot was added to a weighed, fired crucible. Solvent was evaporated, and the residue was calcined at 450°C for 6 hours in air, yielding Mn_5O_8 . This was used to determine the Mn:Cu ratio.

2.1.2 Mn₃O₄ Synthesis

MnO (103 mg, 1.45 mmol) was transferred into a three-neck round bottom flask and hexane was evaporated under vacuum. Degassed 1-octadecene (20 mL) was added to the flask. CuCl₂·2H₂O was added to form a Mn:Cu ratio of 0.4. To achieve a 12:1 N:Cu ratio, degassed oleylamine was added. These ratios were found to be optimal by Varapragasam et al. (our group)²⁰. The flask was fitted with a reflux condenser and the flask was filled with nitrogen to create inert conditions and blanket the solvent. Previous work suggested to react this at 150°C. Instead, the contents were heated to 130°C at a rate of 10°C/min, held for 3 hours, and allowed to cool back to room temperature. Isopropanol (25 mL) was added to precipitate product. This was further isolated by centrifugation at 3500 rpm for 8 minutes. This yielded a dark brown product, and the supernatant was discarded. The nanoparticles were then redispersed in hexanes.

2.2 Catalysis

The hollow Mn₃O₄ nanoparticles were tested for use in catalysis. These NPs were used to attempt to oxidize three different alkenes: cyclohexene, trans-stilbene, and toluene. Cyclohexene was tested in primarily two solvents: THF and hexanes.

2.2.1 Procedure

0.1 mmol of the alkene was added to 1 mL of Mn₃O₄ solution. A 1% catalyst loading was used. For trans-stilbene, tested solvents included tetrahydrofuran (THF), ethanol, hexane, and diethyl ether. For some trials, oxygen was bubbled with a needle into the solution. Bubbling time ranged from 10 minutes to 3 hours. The solution was then refluxed for four, six, or twenty-four, or seventy-two hours in air. If the reaction did not proceed at room temperature, temperatures of 40°F and 60°F were used.

Oxidized products were analyzed with Gas Chromatography Mass Spectrometry (GC-MS) using a Shimadzu GCMS-QP2010 SE. Compounds from the reactions were separated using gas chromatography. A small aliquot (~1 μ L) diluted in ether was injected into the injection port. Helium gas carries the compounds into the capillary column. More volatile compounds and those that poorly interact with the stationary phase (the polysiloxane capillary) elute more quickly. The volatile solvent(s) elute quickly before the ion detector turns on. This avoids overloading the detector. The total ion current (TIC) chromatogram is obtained by summing the intensities of all mass to charge ratios at each retention time.

Mass spectrometry provides mass to charge ratios of ions present in the detector. Electron impact ionization accelerates electrons to 70eV. These electrons impact the eluted compounds which causes fragmentation and ionization. Quadrupole rods separate the ion fragments by mass. The detector converts this into electrical signal which provides the mass spectra at a given retention time.

Two key features of the mass spectra are the molecular ion peak and the base peak. The molecular ion peak tends to have the highest mass to charge ratio. This peak is from the non-fragmented, but ionized molecule. The highest intensity peak (base peak) typically corresponds to the mass to charge ratio of the most stable ion fragment. They provide the most important information for compound identification. However, the pattern and relative intensities of all the mass spec peaks provides a fingerprint for compound identification. The mass spectra are compared with a database of organic molecules to identify each compound in solution.

2.2.2 GC-MS Method File

A new method file was developed with some changes from previous work in our group. The file was entitled “New-R20”. A lower initial temperature was used as cyclohexene oxidation products eluted before the detector was activated. Since a lower temperature was used, a longer initialization time ensured all the solvent passed through the column to avoid overloading the detector. Furthermore, the ramping rate was reduced to 20 degrees per minute to better distinguish the important retention times. Flow rates were automatically adjusted by the program to fit with the new ramping. The mass spectrometry was adjusted to fit the new acquisition time. This was used to analyze the oxidized products of alkenes in GC-MS. Parameters of the New-R20 method file are described below in Figure 2.1 and 2.2.

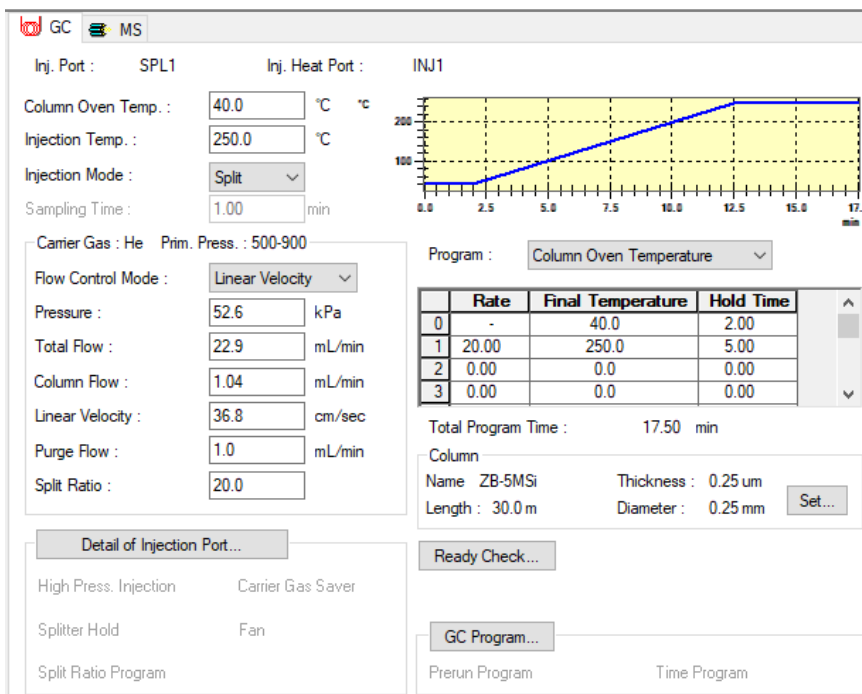


Figure 2.1: Gas Chromatography Method File

GC MS

GCMS-QP2010 with DI

Ion Source Temp.: °C

Interface Temp.: °C Detector Voltage: Relative to the Tuning Result Absolute

Solvent Cut Time: min kV

Micro Scan Width: u Threshold:

Use MS Program: GC Program Time: 17.50 min

Group#1 - Event#1

	Start Time (min)	End Time (min)	Acq. Mode	Event Time(sec)	Scan Speed	Start m/z	End m/z	Ch1 m/z	Ch2 m/z
1	2.00	15.50	Scan	0.50	2000	45.00	1000.00		
2	0.00	0.00	Scan	0.00	0	0.00	0.00		

Figure 2.2: Mass Spectrometry Method File

CHAPTER THREE

Results and Discussion

3.1 Characterization of MnO and Mn₃O₄

Powder X-ray Diffraction (PXRD) is the primary method used to characterize crystalline solids including nanomaterials. The x-rays diffract in a unique pattern based on the crystal lattice of the material. The angle of diffraction and relative intensity provides a unique fingerprint for a given material. Using this technique, the crystallinity and purity can be analyzed.

The diffraction patterns were obtained from a Rigaku Ultima IV instrument. A Cu K α ($\lambda = 1.5406 \text{ \AA}$) radiation source from the X-ray tube was used. The generator was set to 44 kV and 44 mA for data collection. A step size of 0.02° was used for a 2θ scan from 20° to 80° . After purification by precipitation and dispersion, solvent was removed in vacuo. This left a dry powder for diffraction measurements. Figures 3.1 and 3.6 show the diffraction patterns for MnO and hollow Mn₃O₄ nanoparticles, respectively. Crystal lattice planes that align with the 2θ are displayed above the corresponding peaks. These are displayed using the standard (h k l) miller index notation.

Transmission Electron Microscopy (TEM) enables visualization of materials as small as a few hundred atoms across. By capturing images of nanoparticles, the size and shape (morphology) can be studied. Notable features of nanomaterials become apparent, like solidity and surface defects. Uniformity is determined by comparing the individual nanoparticles present in a sample.

Images from Transmission Electron Microscopy (TEM) were taken with a Tecnai Spirit G2 Twin (FEI Company) instrument. LaB6 filament operating at 120 kV was used. Dilute dispersions of nanoparticle samples were drop-casted onto 200 mesh Cu grids with thin film carbon support (Electron Microscopy Sciences). Figure 3.2 contains TEM images of MnO nanoparticles at two different magnitudes. Figure 3.3 contains histogram showing the size of the particles. Hollow Mn₃O₄ nanoparticles are present in Figure 3.4 at two different magnitudes. Figure 3.5 contains three histograms showing the size of the overall nanoparticle (a), the wall thickness (b), and the cavity thickness (c).

3.1.1 MnO NPs

Characterization of the MnO nanoparticles was performed primarily with PXRD and TEM. PXRD shown in Figure 3.1 indicated a highly crystalline nature and a highly pure sample. The spacings and relative intensity match that of MnO. Strong growth along the (2 0 0), (2 2 0), and (1 1 1) crystal planes should be noted.

TEM images, shown in Figure 3.2, seems consistent with the PXRD findings and further indicates a morphology of cubic nature with rounded corners. The MnO nanoparticles are 27.7 ± 3.2 nm wide with a minimum of 18.1 nm and a maximum of 36.4 nm as displayed in Figure 3.3. Notably, these are larger in size than the MnO previously synthesized by our group²¹. The smaller nanoparticles were reported to be unable to form hollow structures upon oxidation. The size change may be due to temperature conditions during reflux.

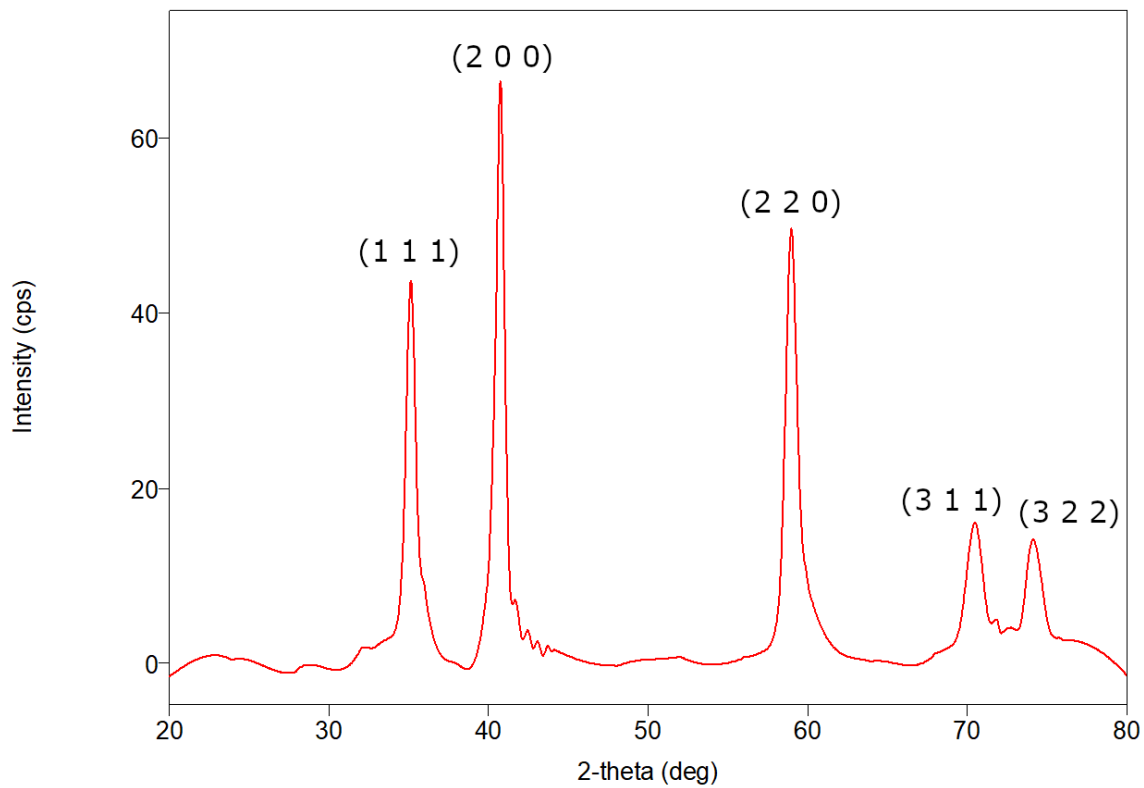


Figure 3.1: PXRD of MnO nanoparticles.

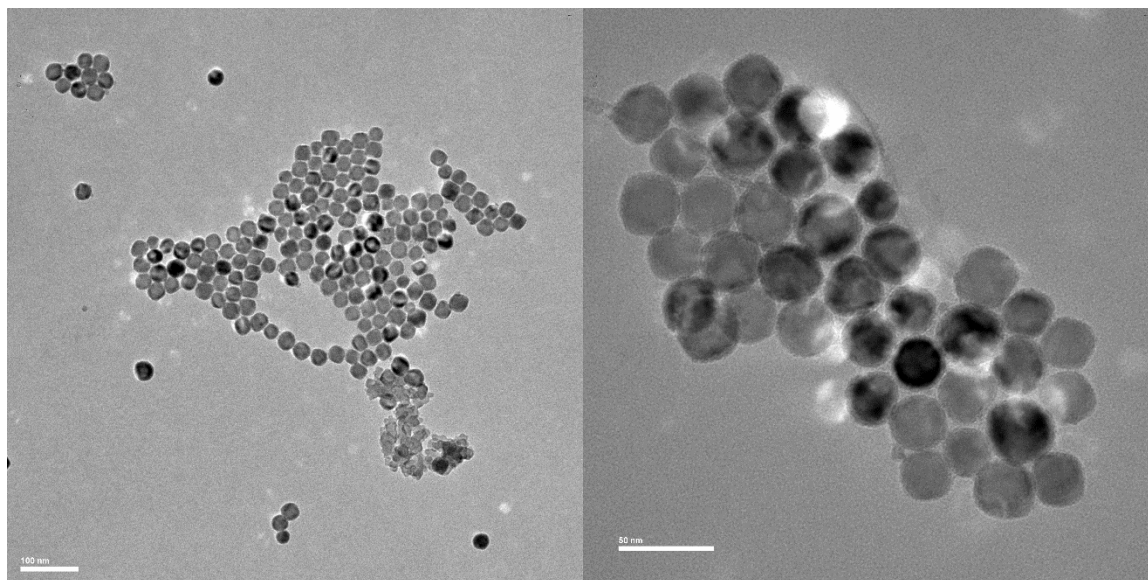


Figure 3.2: TEM of MnO.

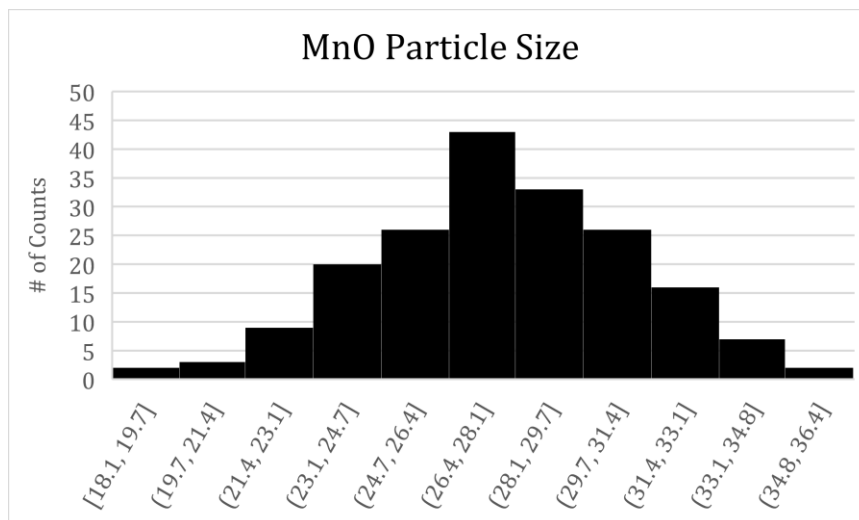


Figure 3.3: Histogram of MnO nanoparticle sizes.

3.1.2 Mn₃O₄ NPs

Characterization of the Mn₃O₄ nanoparticles was performed primarily with PXRD and TEM. PXRD shown in Figure 3.4 indicates high crystallinity. However, the peak at 40° for 2θ clearly indicates the presence of some MnO. Since the smaller MnO nanoparticles retained solid structure under the galvanic reaction, it could be possible that size plays a factor in the galvanic reaction. Notably, this galvanic reaction was reported to deposit Cu in the structure²⁰. Cu makes up between 1.5 and 8% in the hollow Mn₃O₄ structure

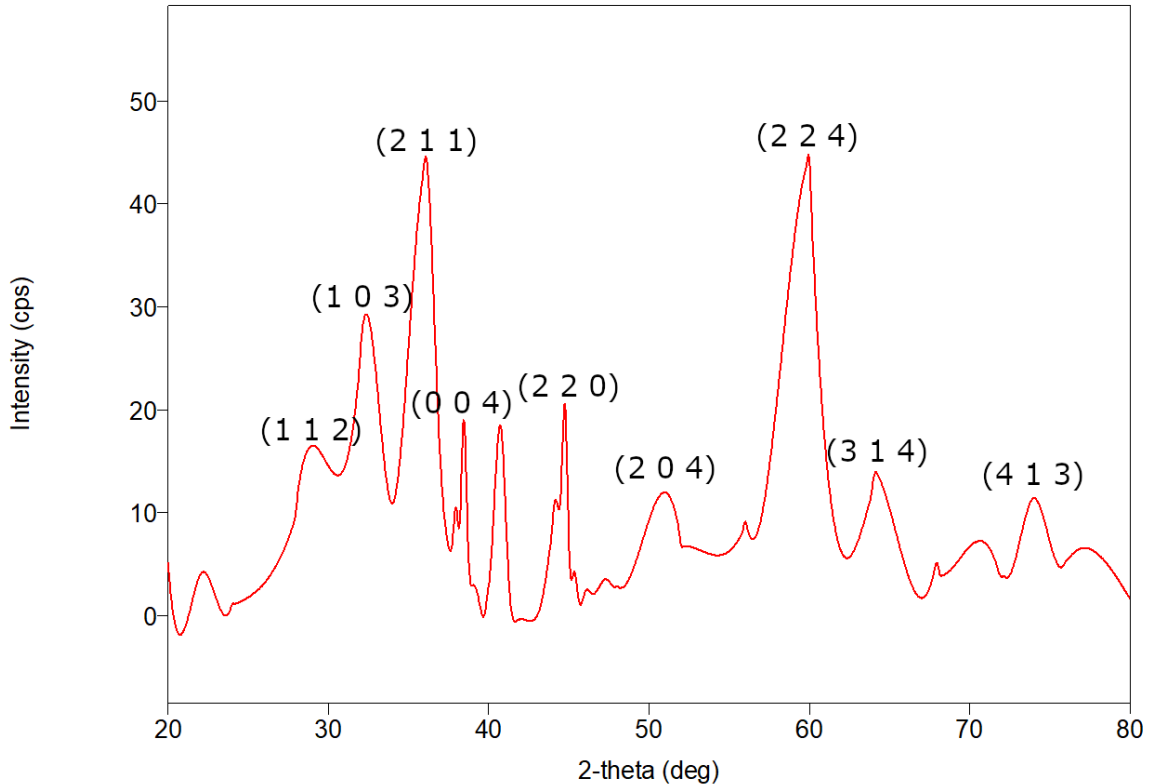


Figure 3.4: PXRD of hollow Mn₃O₄ nanoparticles.

TEM images, shown in Figure 3.5, shows a hollow cubic structure. Figure 3.6 describes some of the dimensions of the hollow nanoparticles. The diameter of the particles is 27.0 ± 3.6 nm with a minimum of 17.8 nm and a maximum of 38.1 nm. The shell

thickness is 6.9 ± 1.3 nm with a minimum of 4.1 nm and a maximum of 10.8 nm (excluding an outlier of 13.6 nm). Lastly, the internal cavity is 12.1 ± 2.7 nm across with a minimum diameter of 5.2 nm and a maximum of 22.1 nm. The shell thickness is consistent with Varapragasam's original results²⁰. The average diameter of the nanoparticles is ~ 3 nm smaller than the original 30 nm particles. Though this result is within the standard deviation, it could be a result of the lowered temperature during the galvanic reaction. Higher temperatures ($>150^\circ\text{C}$) resulted in thermal decomposition. So far, 130°C is used, but lower temperatures could be still tested.

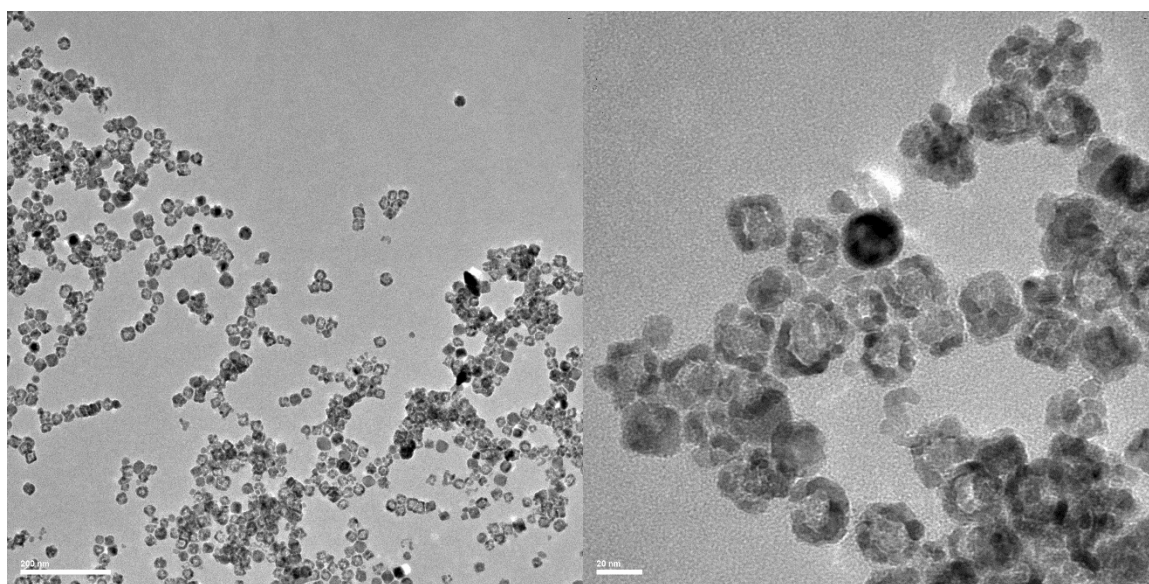


Figure 3.5: TEM of hollow Mn_3O_4 nanoparticles

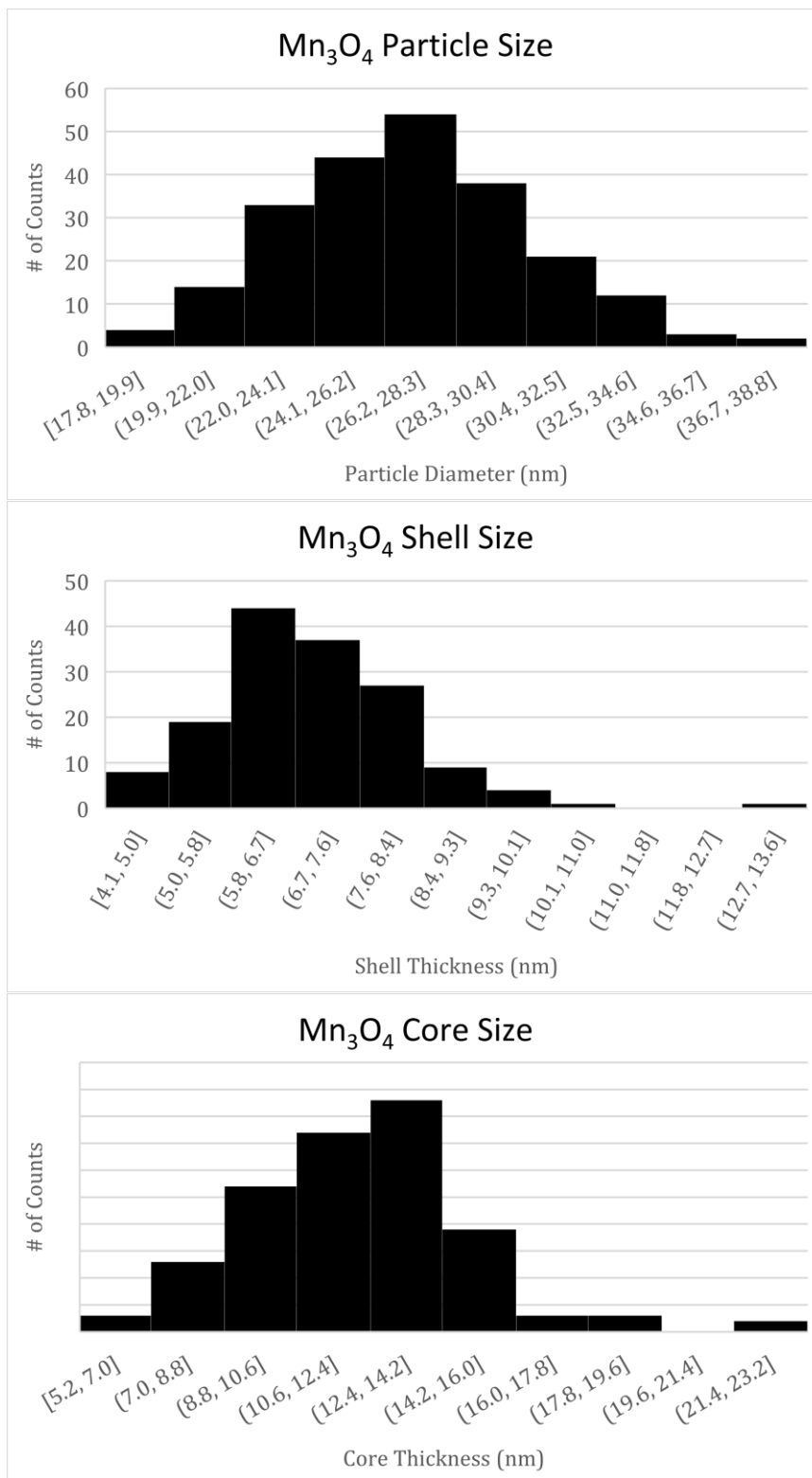


Figure 3.6: Histograms of hollow Mn₃O₄ nanoparticle sizes.
 (a) Full size (b) Wall thickness (c) Core size

3.2 Catalysis Results

3.2.1 Cyclohexene Oxidation

Room temperature oxidation of cyclohexene was performed in hexanes for 24 hours. Figure 3.7a shows the total ion chromatogram for the products from the oxidation. Figures 3.7b-d show the mass spectra for the peaks at retention times of 3.270, 3.347, and 3.715 min, respectively. Table 3.1 indicates the areas under the peaks from GC-MS. Approximately, an 86.9% conversion from cyclohexene can be reported. Furthermore, there is 63.2% selectivity of the ketone product (2-cyclohexen-1-one) over the enol (2-cyclohexen-1-ol). When the reaction is run without the catalyst under the same conditions, a 74.7% conversion is achieved with 69.7% selectivity of the ketone.

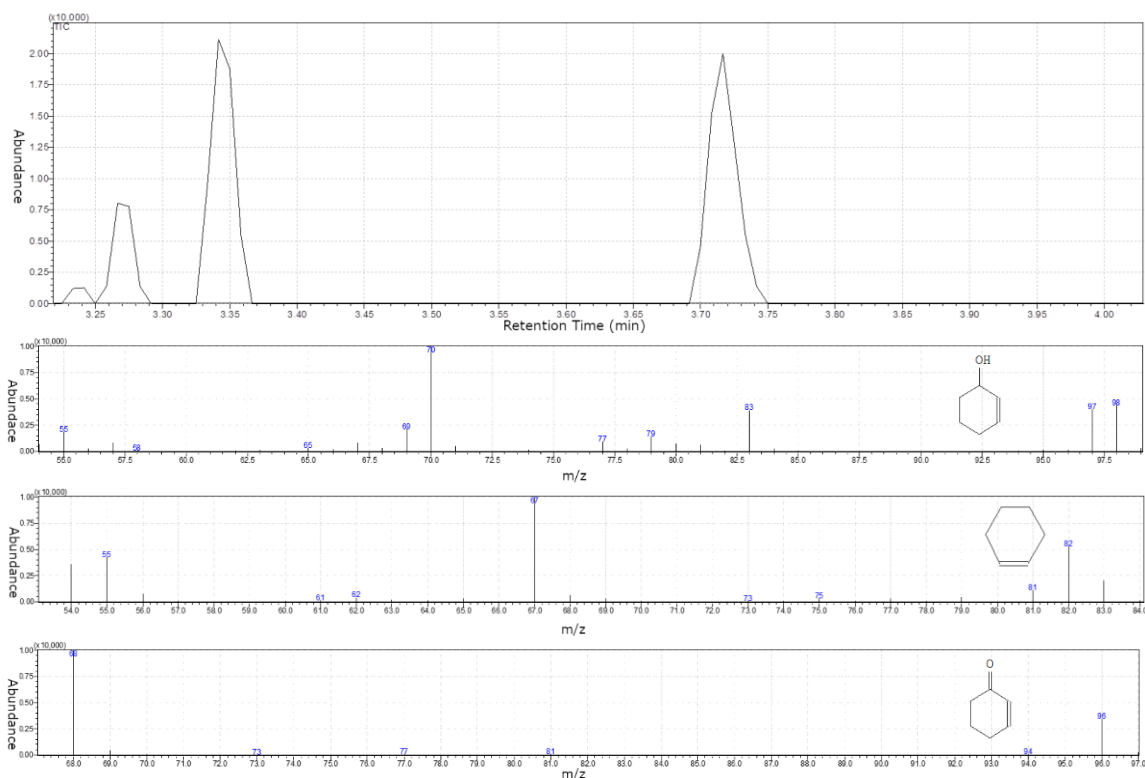


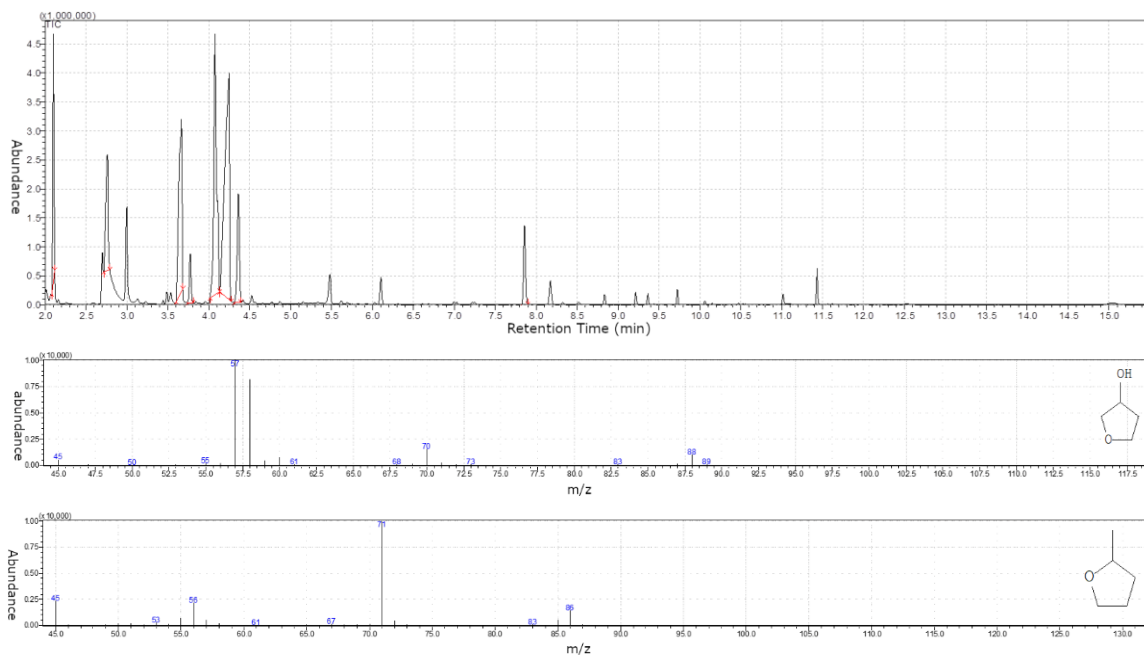
Figure 3.7: GC-MS of Cyclohexene Room Temperature Catalysis in Hexane
(a) Chromatograph of products from reaction of cyclohexene with air (atmospheric oxygen) for 24 hours in hexane. (b) Mass spectra of peak with retention time of 3.270 min. (c) Mass spectra at 3.347 min. (d) Mass spectra at 3.715 min.

Table 3.1: Notable Peaks from Figure 3.7.

Retention, start, and end times are displayed in minutes.

Ret Time	Start	End	Area	Area%	Height	Height%	A/H	Name
3.270	3.225	3.300	117044	28.02	85542	28.79	1.37	2-cyclohexen-1-ol
3.347	3.325	3.400	47990	11.49	34970	11.77	1.37	cyclohexene
3.715	3.683	3.783	201359	48.22	143032	48.14	1.41	2-cyclohexen-1-one

Room temperature oxidation of cyclohexene was performed in tetrahydrofuran (THF) for 24 hours. Figure 3.8a shows the total ion chromatogram for the products from the oxidation. Figures 3.7b-g show the mass spectra for the peaks at retention times of 2.761, 3.664, 3.772, 4.704, 4.362, and 7.858 min, respectively. In THF, the oxidation seems to compete with the solvent. A poorer conversion (45.4%) is achieved than even the control conditions. However, the selectivity of the ketone product is raised to 73.8%. Epoxide, ketone, and hydroxyl products of THF are all formed. Interestingly, of the THF oxidation products, tetrahydro-2-furanmethanol has the highest selectivity (42.1%) as the hydroxyl addition product.



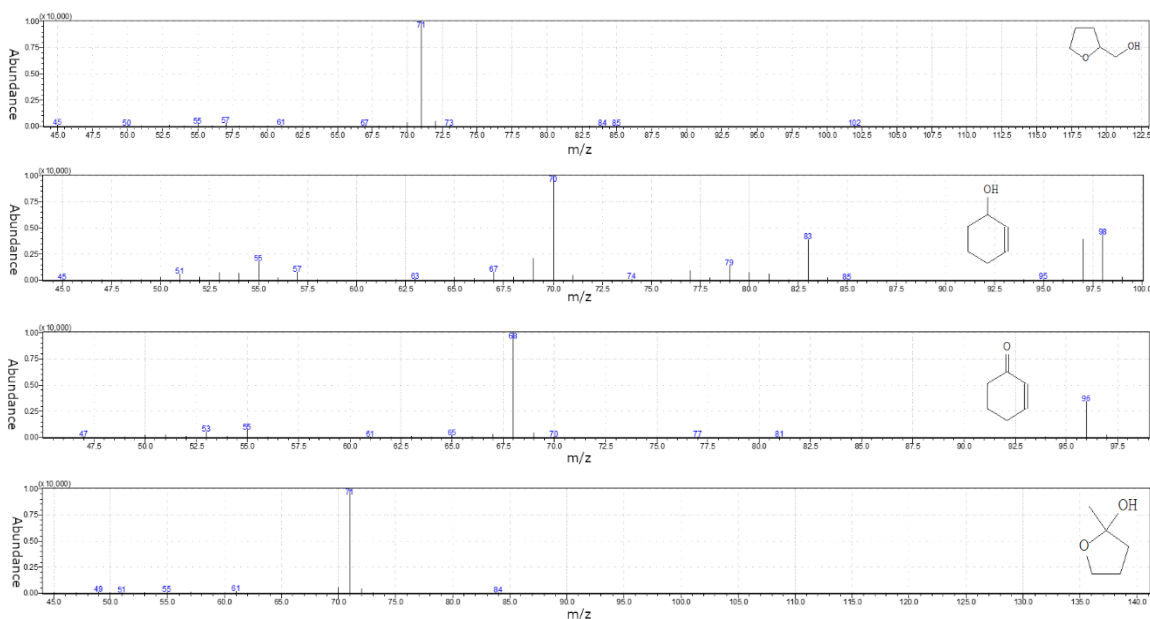


Figure 3.8: GC-MS of Cyclohexene Room Temperature Catalysis in THF

(a) Chromatograph of products from reaction of cyclohexene and THF with air for 24 hours. THF as solvent (b) Mass spectra of peak with retention time of 2.761 min. (c) Mass spectra at 3.664 min. (d) Mass spectra at 3.772 min. (e) Mass spectra at 4.074 min. (f) Mass spectra at 4.362 min. (g) Mass spectra at 7.858 min.

Table 3.2: Notable Peaks from Figure 3.8.

Ret Time	Start	End	Area	Area%	Height	Height%	A/H	Name
2.101	2.083	2.117	4074471	8.29	4270280	19.65	0.95	cyclohexene
2.761	2.717	2.792	4071861	8.29	2001068	9.21	2.03	tetrahydro-3-furanol
3.664	3.600	3.683	8240010	16.77	2984237	13.73	2.76	2-hydroxy-gamma-butylolactone
3.772	3.742	3.808	1281516	2.61	847178	3.90	1.51	2-cyclohexen-1-ol
4.074	4.017	4.133	10456371	21.28	4498128	20.69	2.32	tetrahydro-2-methyl-furan
4.246	4.133	4.275	15217551	30.96	3898227	17.94	3.90	tetrahydro-2-furanmethanol
4.362	4.308	4.392	3610259	7.35	1874599	8.63	1.93	2-cyclohexene-1-one
7.858	7.825	7.900	2186508	4.45	1358594	6.25	1.61	tetrahydro-2-methyl-2-furanol

3.2.2 Trans-Stilbene Oxidation

Oxidation of trans-Stilbene was performed with oxygen bubbled for 30 minutes, then refluxed at 40°C for 24 hours. Figure 3.9a shows the total ion chromatogram for the products from the oxidation. Figure 3.7b shows the mass spectra for the peak at a retention time of 11.74 min. Epoxidation of trans-stilbene does not seem favorable. Only a 1% conversion is achieved. High temp (40°C, 60°C), various solvents, and addition of concentrated O₂ do not seem to increase the favorability of the reaction. In fact, no epoxide products seem to form with our catalyst and conditions for any alkene oxidation.

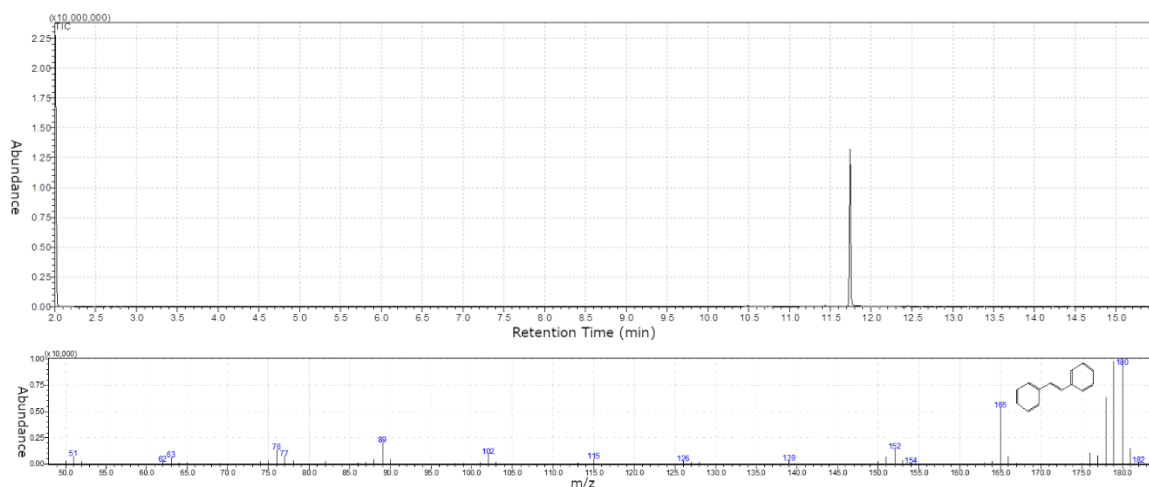


Figure 3.9: GC-MS of Trans-Stilbene 40°C Catalysis with O₂

(a) Chromatograph of products from reaction of trans-stilbene bubbled with O₂ for 30 minutes air and refluxed for 24 hours at 40°C. (b) Mass spectra of peak with retention time of 11.433 min. (c) Mass spectra at 11.741 min.

Table 3.3: Notable Peaks from Figure 3.9.

Ret Time	Start	End	Area	Area%	Height	Height%	A/H	Name
11.433	11.417	11.458	139431	1.01	148055	1.12	0.95	Benzophenone
11.741	11.717	11.767	13678937	98.99	13074707	98.88	2.03	Trans-stilbene

3.2.3 Toluene Oxidation

Room temperature oxidation of toluene was performed with oxygen bubbled for 30 minutes and left in open air for 24 hours. Figure 3.10a shows the total ion chromatogram for the products from the oxidation. Figures 3.10b-d show the mass spectra for the peaks at retention times of 3.638, 3.896, and 4.747 min, respectively. Formation of Benzaldehyde from toluene does occur, but the reaction does not seem very favorable. Ethylbenzene and xylenes (either as impurities or products) are the dominant non-toluene species. Higher temperature or longer times are still able to be tested for this reaction may prove beneficial.

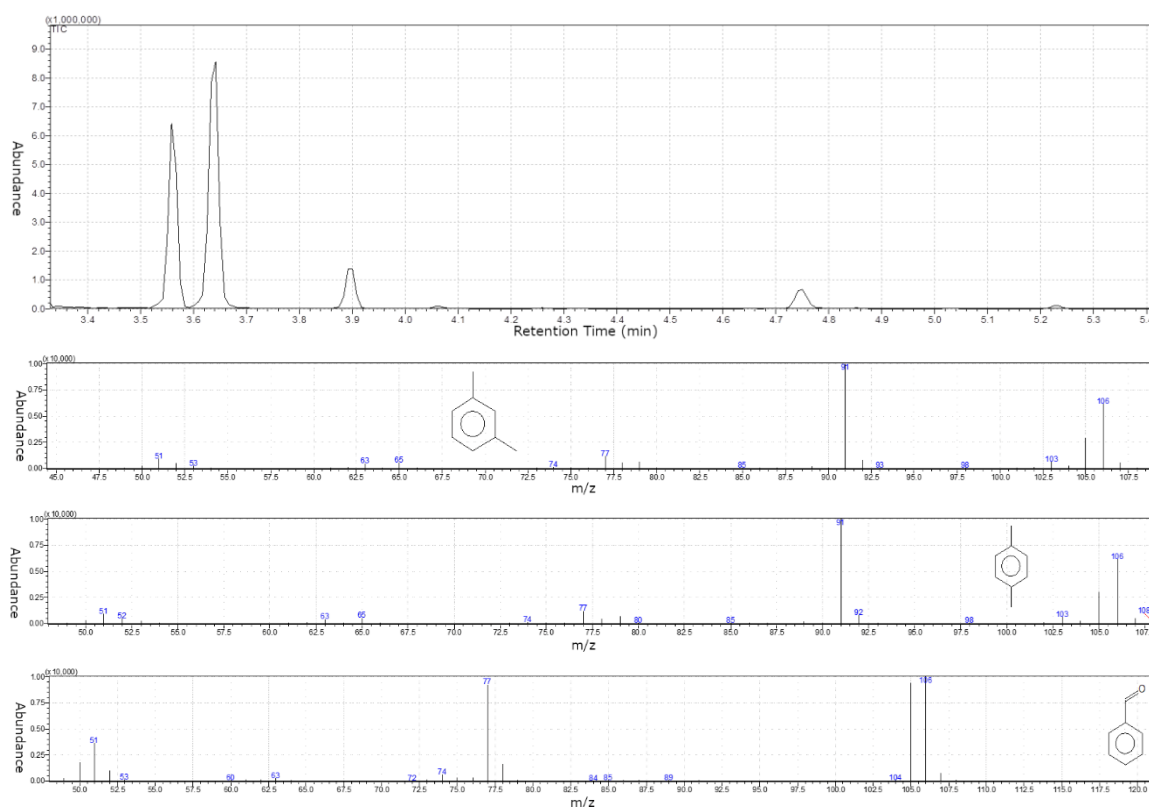


Figure 3.10: GC-MS of Toluene Room Temperature Catalysis with O₂

(a) Chromatograph of products from reaction of toluene bubbled with O₂ for 1 hour and left in open air for 24 hours. (b) Mass spectra of peak with retention time of 3.560 min. (c) Mass spectra at 3.638 min. (d) Mass spectra at 3.896 min. (e) Mass spectra at 4.747 min.

Table 3.4: Notable Peaks from Figure 3.10.

Ret Time	Start	End	Area	Area%	Height	Height%	A/H	Name
3.560	3.517	3.592	7541026	34.21	6397062	37.73	1.18	Ethylbenzene
3.638	3.600	3.683	11548670	52.40	8529375	50.30	1.35	m-xylene
3.896	3.858	3.925	1864477	8.46	1372693	8.10	1.36	p-xylene
4.747	4.717	4.792	1087419	4.93	655466	3.87	1.66	Benzaldehyde

CHAPTER FOUR

Conclusion

Synthesis of hollow Mn_3O_4 nanoparticles have been achieved by first synthesizing MnO nanoparticles followed conversion through galvanic replacement and the Kirkendall effect. Morphology of nanoparticles is dependent on synthetic reaction conditions. These conditions have been slightly optimized by adjusting the reaction temperature conditions. Small changes of temperature can affect the crystal growth.

Initial results for catalytic oxidation of alkenes seems mixed. Many attempted reactions did not proceed. However, a few reactions show initially promising results. In particular, the catalytic oxidation of cyclohexene may prove most useful. While better conversion rates and selectivity are certainly achievable, the cyclohexene reaction is under mild conditions (room temperature, 24 hr). Since the catalyst does not seem to promote epoxidation, it may be useful in alkene oxidation reactions where the epoxide tends to be a minor product.

Further quantitative studies can be performed on these reactions. Once a calibration curve has been established with an internal standard (like hexafluorobenzene), the area can be related to the mols of leftover reactant(s) and products. The oxygen bubbling method likely limits the reactant-catalyst interactions. Better catalyst reaction design engineering may promote improvements to the conversion rate. Mechanistic studies can be performed to determine how the catalyst promotes oxidation. Kinetic studies can also be performed to determine K_{cat} and the turnover number for the catalyst, important to report so our catalyst can be compared to others.

References

- (1) Bharadwaj, S. S.; Schmidt, L. D. CATALYTIC PARTIAL OXIDATION OF NATURAL-GAS TO SYNGAS. *Fuel Process. Technol.* **1995**, *42* (2-3), 109-127. DOI: 10.1016/0378-3820(94)00098-E.
- (2) Lou, B.; Shakoor, N.; Adeel, M.; Zhang, P.; Huang, L.; Zhao, Y.; Zhao, W.; Jiang, Y.; Rui, Y. Catalytic oxidation of volatile organic compounds by non-noble metal catalyst: Current advancement and future perspectives. *J. Clean. Prod.* **2022**, *363*, 132523. DOI: 10.1016/j.jclepro.2022.132523.
- (3) Zhao, G.; Zou, J.; Zhang, T.; Li, C.; Zhou, S.; Jiao, F. Recent progress on removal of indoor air pollutants by catalytic oxidation. *Rev. Environ. Health* **2020**, *35* (4), 311-321. DOI: 10.1515/reveh-2019-0102.
- (4) Wu, M.; Sun, J.; Xiang, W.; Chen, S. Defect engineering in heterogeneous catalytic oxidation catalysts for air pollution elimination: A review of recent progress and strategies. *J. Environ. Chem. Eng.* **2022**, *10* (6), 108734. DOI: 10.1016/j.jece.2022.108734.
- (5) Abatti, D.; Zanicuelli, M. E. D.; Iamamoto, Y.; Idemori, Y. M. Porphyrin LB film as a catalyst for alkene epoxidation. *Thin Solid Films* **1997**, *310* (1), 296-302. DOI: 10.1016/S0040-6090(97)00390-8.

- (6) Lu, H.; Kong, W.; Zhang, C.; Wang, J.; Li, X. The kinetic model of cyclohexene–air combustion over a wide temperature range. *RSC Adv.* **2021**, *11* (63), 39907-39916, 10.1039/D1RA07122J. DOI: 10.1039/D1RA07122J.
- (7) Ghiaci, M.; Aghabarari, B.; Botelho do Rego, A. M.; Ferraria, A. M.; Habibollahi, S. Efficient allylic oxidation of cyclohexene catalyzed by trimetallic hybrid nano-mixed oxide (Ru/Co/Ce). *Appl. Catal. A: Gen.* **2011**, *393* (1), 225-230. DOI: 10.1016/j.apcata.2010.12.006.
- (8) Solé-Daura, A.; Zhang, T.; Fouilloux, H.; Robert, C.; Thomas, C. M.; Chamoreau, L.-M.; Carbó, J. J.; Proust, A.; Guillemot, G.; Poblet, J. M. Catalyst Design for Alkene Epoxidation by Molecular Analogues of Heterogeneous Titanium-Silicalite Catalysts. *ACS Catal.* **2020**, *10* (8), 4737-4750. DOI: 10.1021/acscatal.9b05147.
- (9) Hamidipour, L.; Farzaneh, F. Cobalt metal organic framework as an efficient heterogeneous catalyst for the oxidation of alkanes and alkenes. *React. Kinet. Mech. Catal.* **2013**, *109* (1), 67-75. DOI: 10.1007/s11144-012-0533-2.
- (10) Menini, L.; Pereira, M. C.; Parreira, L. A.; Fabris, J. D.; Gusevskaya, E. V. Cobalt- and manganese-substituted ferrites as efficient single-site heterogeneous catalysts for aerobic oxidation of monoterpenic alkenes under solvent-free conditions. *J. Catal.* **2008**, *254* (2), 355-364. DOI: 10.1016/j.jcat.2008.01.013.
- (11) Maksimchuk, N. V.; Kovalenko, K. A.; Fedin, V. P.; Kholdeeva, O. A. Heterogeneous Selective Oxidation of Alkenes to α,β - Unsaturated Ketones over

Coordination Polymer MIL-101. *Adv. Synth. Catal.* **2010**, *352* (17), 2943-2948. DOI: 10.1002/adsc.201000516.

(12) Maurya, A. Homogeneous catalytic oxidation of alkenes employing mononuclear vanadium complex with hydrogen peroxide. *J. Iran. Chem. Soc.* **2020**, *17* (12), 3261-3269. DOI: 10.1007/s13738-020-01988-x.

(13) Ryan, A. A.; Dempsey, S. D.; Smyth, M.; Fahey, K.; Moody, T. S.; Wharry, S.; Dingwall, P.; Rooney, D. W.; Thompson, J. M.; Knipe, P. C.; et al. Continuous Flow Epoxidation of Alkenes Using a Homogeneous Manganese Catalyst with Peracetic Acid. *Org Process Res Dev* **2023**, *27* (2), 262-268. DOI: 10.1021/acs.oprd.2c00222 From NLM.

(14) Ünver, H.; Kani, I. Homogeneous oxidation of alcohol and alkene with copper (II) complex in water. *J. Chem. Sci.* **2018**, *130* (4), 33. DOI: 10.1007/s12039-018-1439-y.

(15) Fadhel, A. Z.; Pollet, P.; Liotta, C. L.; Eckert, C. A. Combining the benefits of homogeneous and heterogeneous catalysis with tunable solvents and nearcritical water. *Molecules* **2010**, *15* (11), 8400-8424. DOI: 10.3390/molecules15118400 From NLM.

(16) Astruc, D. Introduction: Nanoparticles in Catalysis. *Chem. Rev.* **2020**, *120* (2), 461-463. DOI: 10.1021/acs.chemrev.8b00696.

(17) Koo, B.; Xiong, H.; Slater, M. D.; Prakapenka, V. B.; Balasubramanian, M.; Podsiadlo, P.; Johnson, C. S.; Rajh, T.; Shevchenko, E. V. Hollow Iron Oxide Nanoparticles for Application in Lithium Ion Batteries. *Nano Lett.* **2012**, *12* (5), 2429-2435. DOI: 10.1021/nl3004286.

(18) Nakamura, R.; Tokozakura, D.; Nakajima, H.; Lee, J.-G.; Mori, H. Hollow oxide formation by oxidation of Al and Cu nanoparticles. *J. Appl. Phys.* **2007**, *101* (7). DOI: 10.1063/1.2711383.

(19) Park, J.; An, K.; Hwang, Y.; Park, J.-G.; Noh, H.-J.; Kim, J.-Y.; Park, J.-H.; Hwang, N.-M.; Hyeon, T. Ultra-large-scale syntheses of monodisperse nanocrystals. *Nat. Mater.* **2004**, *3* (12), 891-895. DOI: 10.1038/nmat1251.

(20) Varapragasam, S. J. P.; Balasanthiran, C.; Gurung, A.; Qiao, Q.; Rioux, R. M.; Hoefelmeyer, J. D. Kirkendall Growth of Hollow Mn₃O₄ Nanoparticles upon Galvanic Reaction of MnO with Cu²⁺ and Evaluation as Anode for Lithium-Ion Batteries. *J. Phys. Chem. C* **2017**, *121* (21), 11089-11099. DOI: 10.1021/acs.jpcc.7b01540.

(21) Dhali, B. K. S. Selective oxidation of alkenes in air catalyzed by Mn₃O₄ nanoparticles. *Dissertations and Theses* **2021.**, *18*.